Journal of ELECTRONIC MATERIALS, Vol. 40, No. 5, 2011
DOI: 10.1007/s11664-011-1548-6

Enhancing Thermoelectric Properties of Polycrystalline Bi_2S_3 by Optimizing a Ball-Milling Process

ZHEN-HUA GE,[1] BO-PING ZHANG,[1,3] PENG-PENG SHANG,[1] YI-QIANG YU,[1] CHEN CHEN,[1,2] and JING-FENG LI[2]

1.—Beijing Key Lab of New Energy Materials and Technology, School of Materials Science and Engineering, University of Science and Technology Beijing, Beijing 100083, China. 2.—State Key Laboratory of New Ceramics and Fine Processing, Department of Materials Science and Engineering, Tsinghua University, Beijing 100084, China. 3.—e-mail: bpzhang@ustb.edu.cn

Bismuth sulfide (Bi_2S_3) polycrystalline samples were fabricated by mechanical alloying (MA) combined with spark plasma sintering (SPS). The microstructure and electrical transport properties were investigated with special emphasis on the influence of the ball-milling process. Bi_2S_3 compound powders could be readily synthesized directly from elemental powders under all the investigated conditions, and highly dense *n*-type bulk Bi_2S_3 samples with high density (>95%) were fabricated by the subsequent SPS process. Changing the MA conditions had no apparent influence on the microstructure or phase structure of the MA-derived Bi_2S_3 powders, but the electrical properties and thermopower of the SPS-sintered Bi_2S_3 bulk samples were greatly dependent on the MA speed and time. The power factor of Bi_2S_3 was increased to 233 $\mu W\ K^{-2}\ m^{-1}$ at 573 K by optimizing the ball-milling process. This power factor is higher than values reported to date for Bi-S binary samples without texture.

Key words: Bi_2S_3, thermoelectric, mechanical alloying, ball-milling process

INTRODUCTION

Solid-state thermoelectric (TE) power generators possess many advantages, such as silent operation, reliability, and scalability, which therefore make them ideal for distributed waste-heat harvesting. The efficiency of TE devices is determined by the dimensionless figure of merit (ZT), defined as $ZT = S^2\sigma T/\kappa$,[1,2] where S, σ, T, and κ are the Seebeck coefficient, electrical conductivity, absolute temperature, and thermal conductivity, respectively. Bismuth telluride (Bi-Te)-based compounds show the best TE properties near room temperature. Although Te-based materials usually exhibit good TE properties and represent a dominant market share of TE materials, it is necessary to develop alternative materials to replace the rare and toxic tellurium. Bismuth sulfide (Bi_2S_3) belongs to the A_2B_3-type (A = Bi, Sb, Pb; B = S, Se, Te) compounds and is a layered semiconductor with a direct band gap ($E_g \approx 1.3$ eV). The phase structure is in the orthorhombic system (*pbnm* space group) and is isostructural to Sb_2S_3 and Sb_2Se_3.[3] The electrical resistivity of Bi_2S_3 is about two orders of magnitude higher than that of Bi_2Te_3 compounds. In 1917, Case[4] first reported the photoconductivity of Bi_2S_3 in bismuthinite or bismuth glance mineral samples. G. Hodes and coworkers[5] studied the conductivity and photoconductivity of some ternary and pseudo-binary Bi_2S_3 compounds. Chen et al.[6] first reported the thermoelectric properties of Bi_2S_3, which was proposed as a good TE material because of its high Seebeck coefficient (about 500 $\mu V\ K^{-1}$) and low thermal conductivity (<1 $W\ m^{-1}\ K^{-1}$), in which the lattice thermal conductivity plays the dominant role due to the low carrier concentration and the high resistivity. We also found that Bi_2S_{3-x} polycrystalline materials prepared by MA and SPS have a very low thermal conductivity (about 0.5 $W\ m^{-1}\ K^{-1}$ to 0.8 $W\ m^{-1}\ K^{-1}$).[7] It seems that, even though the electrical conductivity of SPS-sintered Bi_2S_3 was improved, the thermal conductivity was not

(Received May 28, 2010; accepted January 24, 2011; published online March 1, 2011)

dramatically increased and remained at a low level. Hence, decreasing the resistivity conductivity and enhancing the power factor are the major approaches to improve the TE properties, rather than tailoring the thermal conductivity. Much effort has been invested in synthesis of one-dimensional Bi_2S_3 by chemical and physical routes, including the hydrothermal method,[8] chemical vapor deposition (CVD),[9] electrochemical deposition,[10] microwave irradiation,[11] as well as the solvothermal method,[12] while little attention has been paid to bulk Bi_2S_3.

Mechanical alloying (MA) is superior to conventional melting or grinding techniques for fabricating nanosized alloys.[13] Spark plasma sintering (SPS) is suitable for fabricating TE materials, since this technique can restrict grain growth owing to its low sintering temperature and short sintering time. Recently, Zhao et al.[14] fabricated high-performance Bi_2Te_3-based materials by the MA and SPS techniques, reporting a maximum ZT value of 1.18 at 423 K, which confirms MA plus SPS as a simple and effective method to prepare TE materials even with complex compositions. In the present work, Bi_2S_3 bulk samples were synthesized by the MA and SPS techniques, and the microstructure and electrical transport properties were investigated with special emphasis on the influence of ball-milling parameters. As a result, a maximum power factor of 233 $\mu W\ K^{-2}\ m^{-1}$ was obtained at 573 K, being higher than values reported to date for the pure-phase nontextured bulk Bi_2S_3 system.[7]

EXPERIMENTAL PROCEDURES

Commercial high-purity powders of Bi (99.9%) and S (99.9%) under the same 100 mesh were used as raw materials. Powders with chemical composition of Bi_2S_3 were subjected to MA at 350 rpm to 450 rpm for 15 h to 25 h in an atmosphere of argon (95%) and hydrogen (5%) gas mixture using a planetary ball mill (QM-1SP2, China), and then to MA at 250 rpm for 1 h in an alcohol liquid. Here, a stainless-steel vessel and balls were used, and the weight ratio of balls to powder was kept at 20:1. The mechanically alloyed powders were loaded into a graphite die with an inner diameter of 20 mm, and then sintered at 673 K for 5 min under an axial compressive stress of 40 MPa in vacuum by using a SPS system (SPS1050; Sumitomo, Japan). The SPS-sintered specimens were disk-shaped with dimensions of Ø20 mm × 4 mm. The phase structure was analyzed by x-ray diffraction (XRD, Bruker D8, Germany) with Cu Kα radiation. The morphologies of powders and the fracture of bulk samples were observed by field-emission scanning electron microscopy (FESEM, SUPRA™ 55, Japan). The electrical transport properties were evaluated along a sample section perpendicular to the SPS pressing direction. The Seebeck coefficient and electrical resistivity were measured from 323 K to 573 K in helium atmosphere using a Seebeck coefficient/electrical resistance measuring system (ZEM-2 Ulvac-Riko, Japan). The density (d) of the sample was measured by the Archimedes method. In addition, the thermal conductivity of the sample with the highest power factor was calculated by the relationship $k = DC_pd$ from the thermal diffusivity D measured by the laser flash method (LFA427; NETZSCH, Germany), specific heat (C_p), and density d.

RESULTS

Figure 1 shows XRD patterns of Bi_2S_3 powders that were subjected to MA with different milling parameters (350 rpm to 450 rpm for 15 h to 25 h). Varying the milling speed from 350 rpm to 450 rpm for a constant milling time (15 h), as shown in Fig. 1a, all the diffraction peaks for the samples correspond well to those of Bi_2S_3 (*PDF#17-0320*) without any detectable second phase(s), which suggests that a single Bi_2S_3 phase with orthorhombic symmetry was synthesized during the MA process. Figure 1b highlights the XRD pattern of the diffraction peak in the 2θ range from 24° to 26°. Although there are two diffraction lines (130) and (310) corresponding to 24.93° and 25.21° in the standard card (*PDF#17-0320*), only one broad diffraction peak is observed in all the powder samples. This can be explained by considering that the powder grains are too small to allow separation of the (130) and (310) peaks in the XRD measurements. Fixing the milling speed at 425 rpm and varying the milling time from 15 h to 20 h and 25 h, the XRD patterns in Fig. 1c and d for the Bi_2S_3 powders show a similar trend to those in Fig. 1a and b. All the powders (Fig. 2c) are also in a pure phase, and the (130) and (310) diffraction peaks in Fig. 2d are barely distinguishable from each other.

Figure 2 shows XRD patterns of Bi_2S_3 bulk material obtained by applying SPS to powders mechanically alloyed using different milling parameters (350 rpm to 450 rpm for 15 h to 25 h). The diffraction peaks of the bulk materials are sharper than those of the powder samples (Fig. 1a, c), corresponding to a single phase that matches the pattern for binary Bi_2S_3 (*PDF#17-0320*) for all the bulk materials and powders, which is attributed to enhanced crystallinity due to the SPS process. The (130) and (310) diffraction peaks in Fig. 2b, which overlapped for the powder samples in Fig. 1b, d, now become distinguishable due to grain growth. The 2θ angles of the (130) peaks with the highest diffraction intensity, which are lower than the angle of the peak (24.93°) in the standard card, exhibit a shift towards lower diffraction angle that increases with increasing milling speed. This peak shift to lower diffraction angle indicates enlargement of the Bi_2S_3 crystals. A similar shift behavior of diffraction angle with decreasing sulfur content was also found previously in polycrystalline Bi_2S_{3-x} (x = 0, 0.05, 0.1, 0.15) prepared using the same MA and SPS

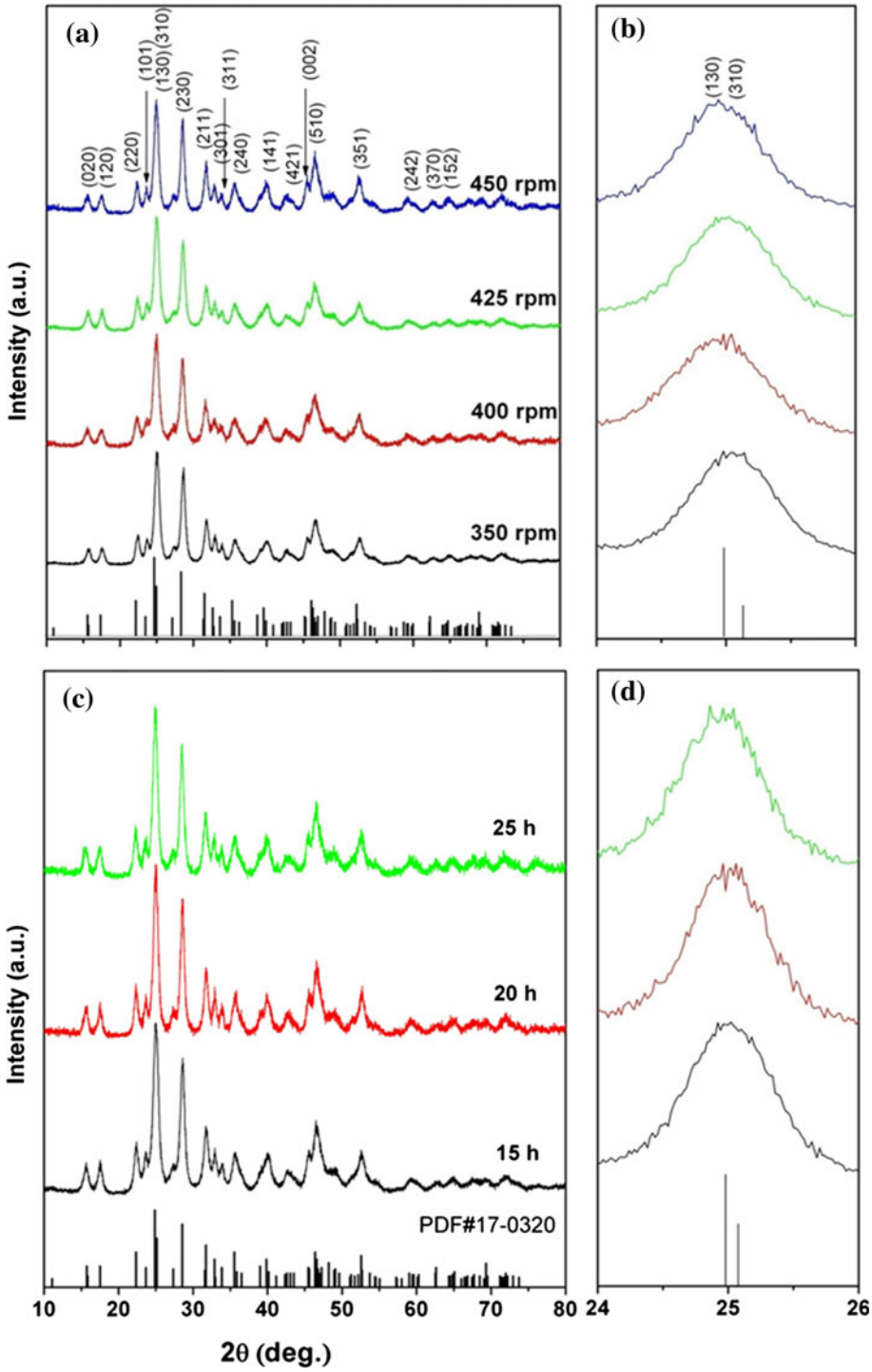

Fig. 1. XRD patterns of Bi_2S_3 powders subjected to MA at 350 rpm to 450 rpm for 15 h (a, b) and at 425 rpm for 15 h to 20 h (c, d).

conditions.[7] This suggests that the as-fabricated Bi_2S_3 bulk material was sulfur deficient, caused by volatilization of sulfur, which has a lower melting point (388.2 K) than that of bismuth (544.4 K). The increasing sulfur vacancies with milling speed in the SPS-sintered bulk materials could be related to varying microstructure of the bulk samples, since the subsequent SPS conditions were the same for all the samples, as discussed below. XRD patterns of bulk samples obtained by using powder subjected to MA at a constant milling speed of 425 rpm for different milling times (15 h, 20 h, and 25 h) are shown in Fig. 2c, d. All the bulk materials were also in a pure phase, similar to the trend shown in

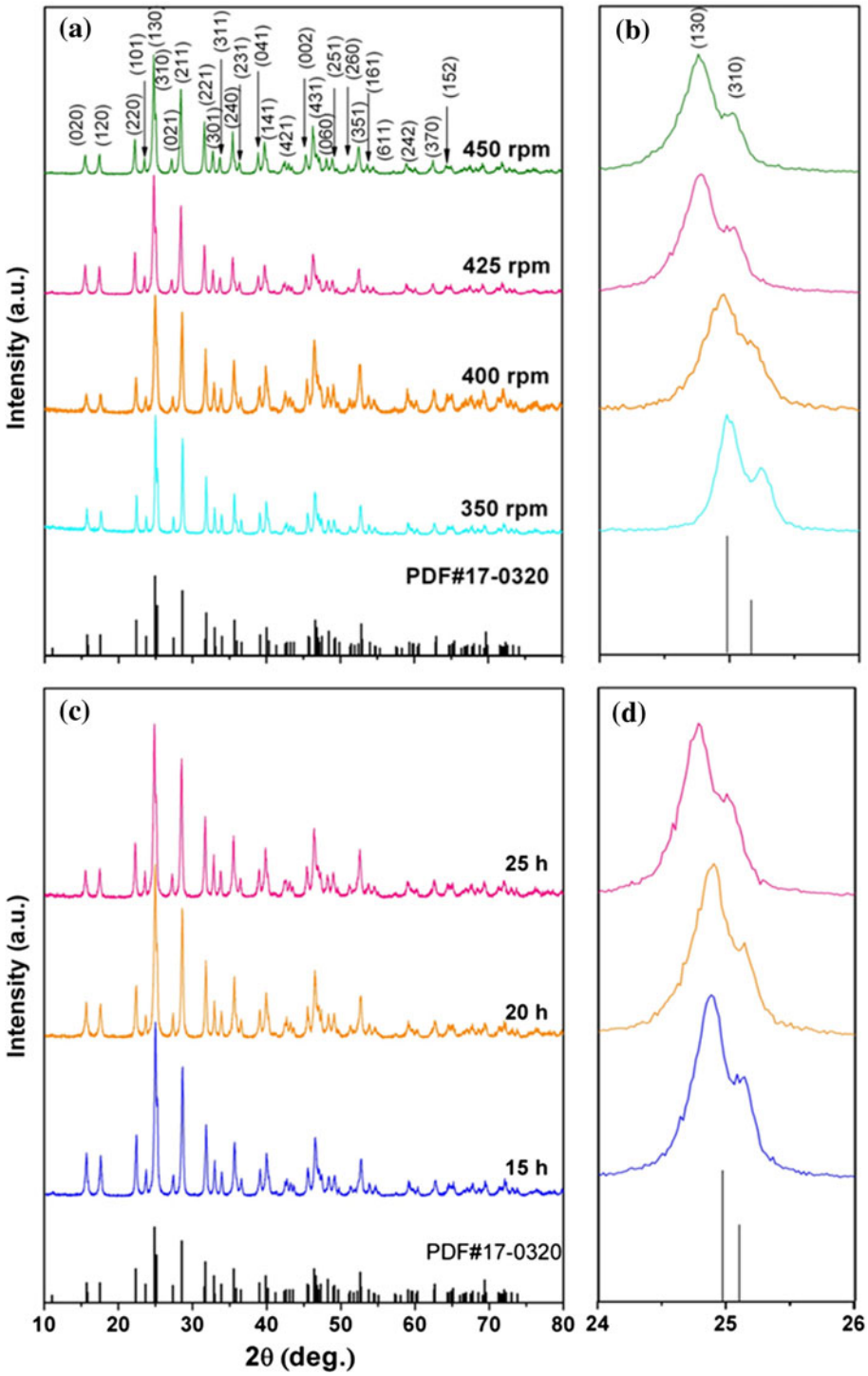

Fig. 2. XRD patterns of Bi_2S_3 bulk material obtained by applying SPS at 673 K for 5 min to powders mechanically alloyed at 350 rpm to 450 rpm for 15 h (a, b) and at 425 rpm for 15 h to 20 h (c, d).

Fig. 2a, b. The 2θ angles of the (130) peaks in Fig. 2d are 24.74°, 24.72°, and 24.68° for SPS-sintered samples obtained from powders milled for 15 h, 20 h, and 25 h, respectively, indicating that the shift of the diffraction peak caused by the increase of the sulfur vacancies also appears in the bulk samples with increasing milling time.

Figure 3 shows FESEM micrographs of fractured surfaces of Bi_2S_3 bulk material obtained by applying SPS at 673 K for 5 min to powders that were mechanically alloyed with different milling speeds and times. The samples show a dense microstructure with a relative density above 95%. The grain sizes of all the samples are about 200 nm to 500 nm

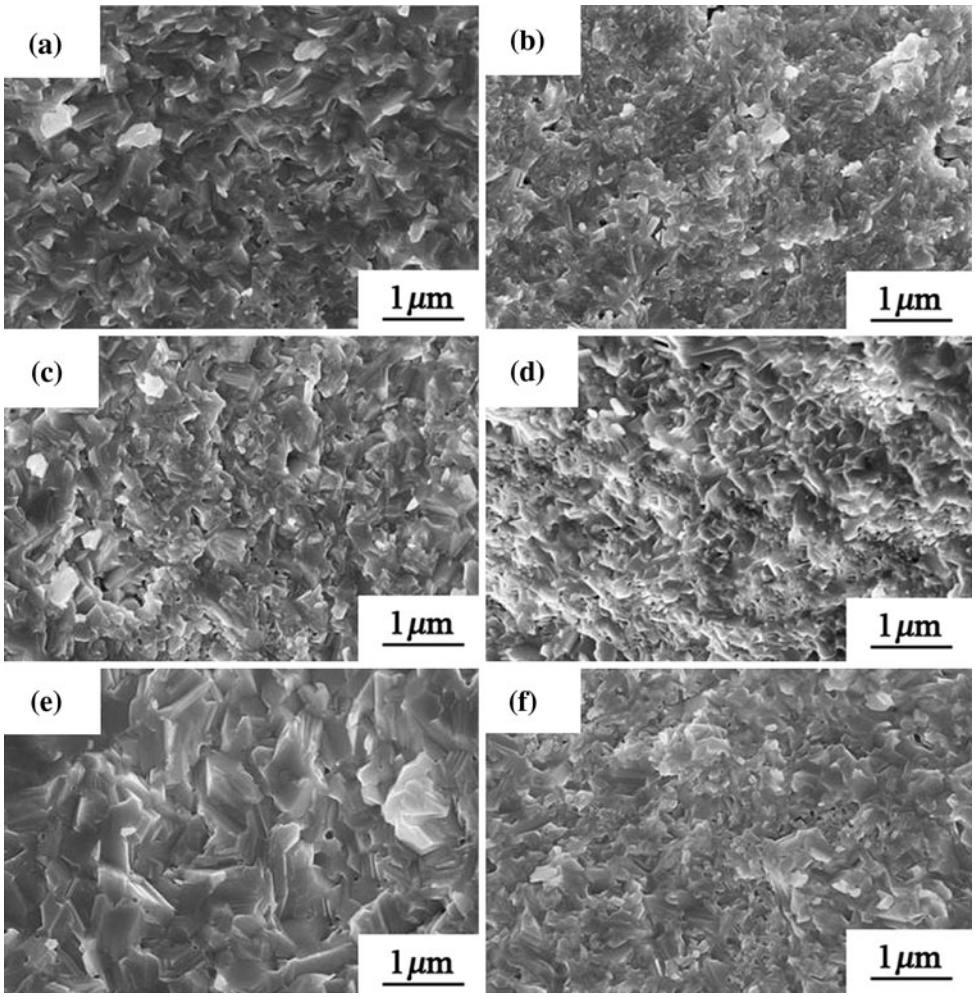

Fig. 3. FESEM micrographs of Bi_2S_3 bulk materials obtained by applying SPS at 673 K for 5 min to powders subjected to MA for 15 h at 300 rpm (a), 400 rpm (b), 425 rpm (c), and 450 rpm (d), as well as at 425 rpm for 20 h (e) and 25 h (f).

and grow gradually with increasing milling speed. However, the grain sizes decrease as the rotation speed is further raised from 425 rpm to 450 rpm for a constant milling time (15 h). As shown in Fig. 3a–d, the average grain size of the samples is about 200 nm, 250 nm, 300 nm, and 260 nm for bulk materials obtained by applying SPS to precursor powders mechanically alloyed at 350 rpm, 400 rpm, 425 rpm, and 450 rpm for 15 h, respectively. A similar trend of variation of grain size is more obvious for different milling times, as shown in Fig. 3c, e, f. The bulk samples obtained from powders subjected to MA at 425 rpm for 20 h showed the largest grain size (~500 nm) among all the samples.

Figure 4 shows the temperature dependence of the electrical transport properties for Bi_2S_3 bulk material obtained by applying SPS at 673 K for 5 min to powders subjected to MA with different milling speeds (350 rpm to 450 rpm) for 15 h. As shown in Fig. 4a, the electrical resistivity of all the bulk samples decreases with increasing temperature, indicating semiconducting behavior. The electrical resistivity of the bulk samples decreases in the measuring temperature range from 323 K to 573 K with increasing milling speed from 350 rpm to 425 rpm. However, the electrical resistivity increases again when the milling speed is further increased from 425 rpm to 450 rpm.

Figure 4b shows the variations of the Seebeck coefficient as a function of measuring temperature for Bi_2S_3 bulk materials. The negative Seebeck coefficient values indicate that all the samples are *n*-type and the majority carrier is the electron. All samples showed a decreasing trend with measuring temperature, which is inversely related to the variations of the electrical conductivity with temperature. The Seebeck coefficient for bulk samples obtained by applying SPS to powders subjected to MA at 350 rpm for 15 h shows the highest values of about $-500\ \mu V\ K^{-1}$ to $-490\ \mu V\ K^{-1}$ at 323 K to 573 K, consistent with results reported elsewhere.[12] As the milling speed increased from 350 rpm to 400 rpm and 425 rpm, the Seebeck coefficient at

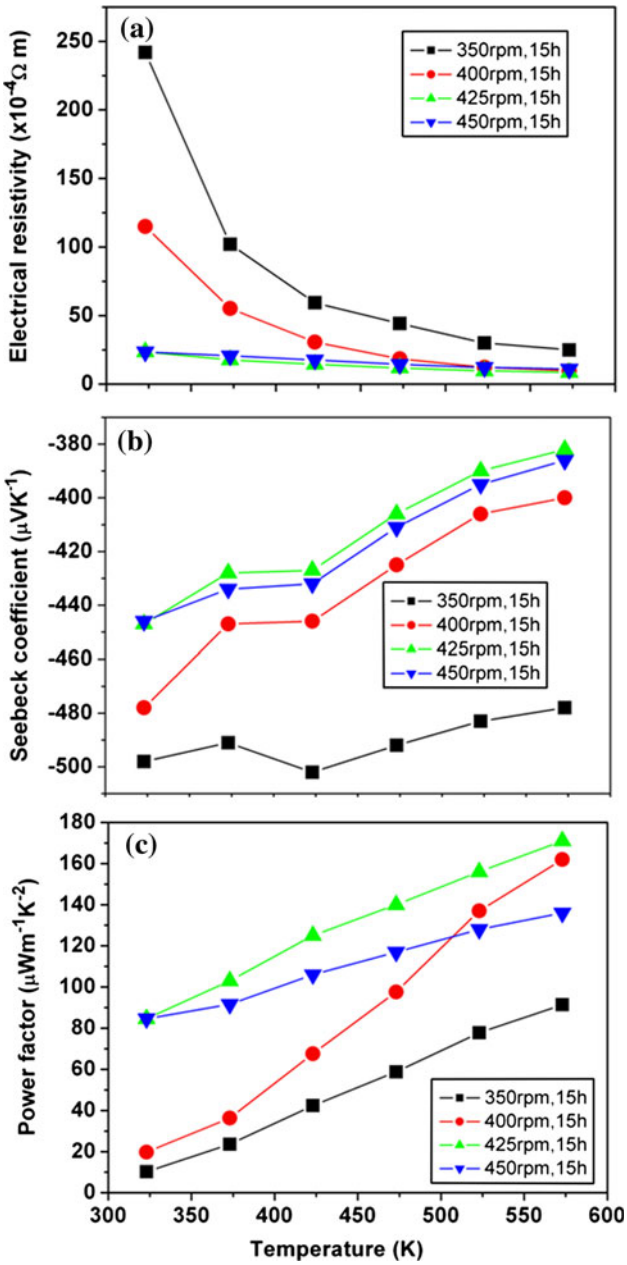

Fig. 4. Temperature dependence of electrical resistivity (a), Seebeck coefficient (b), and power factor (c) for Bi_2S_3 bulk material obtained by applying SPS at 673 K for 5 min to powders subjected to MA at 350 rpm to 450 rpm for 15 h.

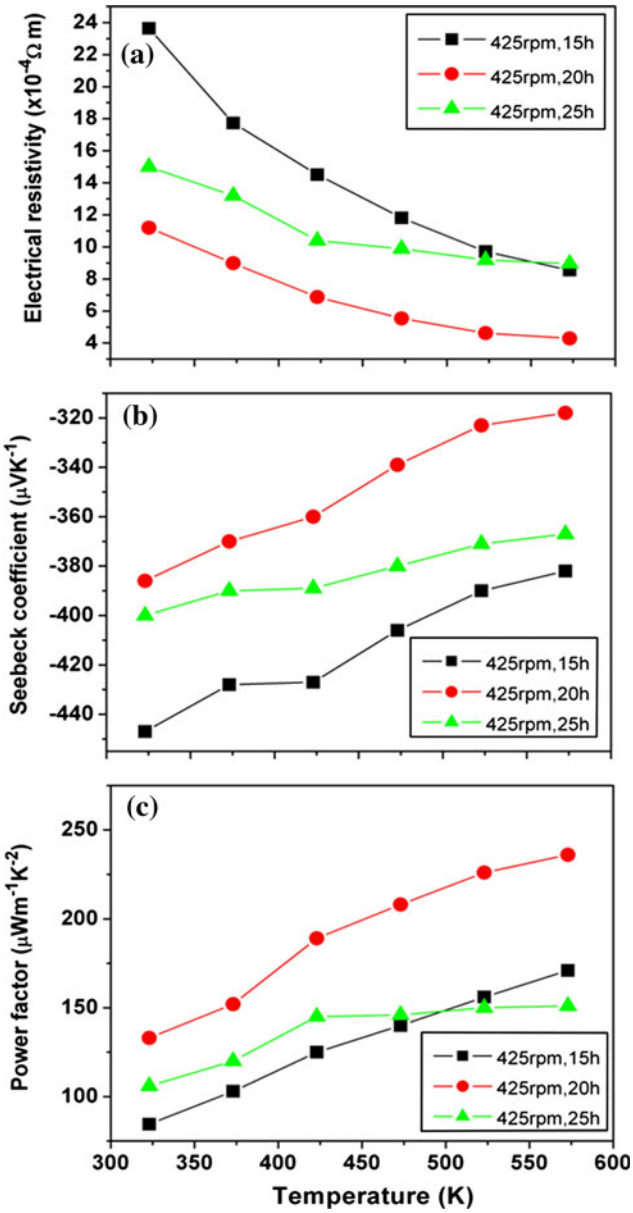

Fig. 5. Temperature dependence of electrical resistivity (a), Seebeck coefficient (b), and power factor (c) for Bi_2S_3 bulk materials obtained by applying SPS to powder mechanically alloyed at 425 rpm for 15 h to 25 h.

room temperature further decreased to −478 μV K^{-1} and −447 μV K^{-1}. The corresponding power factor as a function of measuring temperature for the bulk samples shows an increasing trend with measuring temperature (Fig. 4c). When the powder was milled at 350 rpm, the bulk material had the lowest power factor, ranging from 10 μW m^{-1} K^{-2} to 80 μW m^{-1} K^{-2} for temperatures from 323 K to 573 K. The power factor increases with increasing ball-milling speed, reaching 173 μW m^{-1} K^{-2} at 573 K at 425 rpm, which is about twice as high as the reported value (91 μW m^{-1} K^{-2}).[7]

Figure 5 shows the temperature dependence of the electrical transport properties for Bi_2S_3 bulk materials obtained by applying SPS to powders subjected to MA for different milling times (15 h to 25 h) at the optimal milling speed of 425 rpm. As shown in Fig. 5a, the electrical resistivity of all the bulk samples decreases with increasing temperature because of the semiconducting behavior. When the milling time was fixed at 20 h, the electrical resistivity of the bulk materials was about 1.2 × 10^{-3} Ω m at room temperature, which is half that for the bulk sample obtained by applying SPS to powder milled for 15 h. Further ball-milling of the

powders from 20 h to 25 h caused an increase in the electrical resistivity over the whole measurement temperature range.

Figure 5b shows the variations of the Seebeck coefficient as a function of temperature. The negative Seebeck coefficient values indicate that all the samples are *n*-type and the majority carrier is the electron. The Seebeck coefficient for bulk Bi_2S_3 samples obtained from applying SPS to powders subjected to MA at 425 rpm for 15 h shows the highest values of about $-450\ \mu V\ K^{-1}$ to $-390\ \mu V\ K^{-1}$ at 323 K to 573 K. A decreasing trend in the Seebeck coefficient appears as the milling time is prolonged to 20 h. When the milling time was further prolonged from 20 h to 25 h, the Seebeck coefficient increases inversely. The corresponding power factor shown in Fig. 5c is enhanced with increasing milling time from 15 h to 20 h and reaches $233\ \mu W\ m^{-1}\ K^{-2}$ at 573 K, the highest value reported so far for pure and nontextured polycrystalline Bi_2S_3.

DISCUSSION

MA is a solid-state powder processing technique involving repeated welding, fracturing, and rewelding of powder particles in a high-energy ball mill, which is capable of synthesizing a variety of equilibrium and nonequilibrium alloy phases starting from blended elementals or pre-alloyed powders.[15] The ball-milling speed and time are the most important parameters, and both of them determine the energy input into the powder based on the following equation:[16]

$$E = K\omega^n t, \tag{1}$$

where E, K, n, ω, and t are the necessary energy in certain states of powders in MA process, the energy for one collision, an index, the milling speed, and the milling time, respectively. Therefore, either increasing the milling speed or prolonging the milling time can provide more energy to refine powders that require a reduced densification temperature. Grain growth is more apparent when powders are milled at higher speed for longer time, for the same sintering temperature. However, heavily refined powders tend to contain more sulfur vacancies ($V_s^{\bullet\bullet}$) in MA and SPS processes, and excessive $V_s^{\bullet\bullet}$ can prevent grain growth, as shown in Fig. 3d, f. As a result, the bulk sample using powder milled at 425 rpm for 20 h shows the largest grain size (Fig. 3e). On the other hand, powder refinement and activation by increasing the milling speed or prolonging the milling time also tend to aggravate sulfur volatilization during the subsequent SPS process, whereby traces of sulfur volatilization appear for the SPS-sintered bulk (Fig. 2) but not for powder that was previously subjected to MA (Fig. 1).

In the SPS process under the same sintering conditions (673 K for 5 min) after the MA step, volatilization of sulfur depends on the initial state of the powder. Reduction of a sulfur atom in Bi_2S_3 generates $V_s^{\bullet\bullet}$ to increase the number of electrons, as described by the following equation:

$$Bi_2S_3 \rightarrow Bi_2S_{3-x} + xS_g \uparrow + xV_s^{\bullet\bullet} + 2xe' \tag{2}$$

The resulting electron (e′) generated by the $V_s^{\bullet\bullet}$ causes an increase in the carrier (electron) concentration for *n*-type materials.

The electrical resistivity and Seebeck coefficient are expressed by the following two equations:

$$\rho = 1/\mu ne, \tag{3}$$

$$S \approx \gamma - \ln n, \tag{4}$$

where ρ, μ, n, S, and γ are the electrical resistivity, carrier mobility, carrier concentration, Seebeck coefficient, and scattering factor, respectively. The electrical resistivity is inversely proportional to the carrier mobility and the carrier concentration, whereas the Seebeck coefficient is proportional to the scattering factor and inversely proportional to the carrier concentration.[17] Therefore, the increase in carrier concentration obtained by increasing the milling speed and/or prolonging the milling time contributes to decrease both the electrical resistivity (Figs. 4a, 5a) and the Seebeck coefficient (Figs. 4b, 5b), resulting in enhancement of the power factor. In Figs. 4 and 5, the electrical resistivity of the bulk samples decreases with increasing milling speed from 350 rpm to 425 rpm for 15 h or increasing milling time from 15 h to 20 h at 425 rpm, which is due to increased carrier concentration and grain growth. However, further increase of either the milling speed to 450 rpm or milling time to 25 h increases the electrical resistivity, which may be due to microstructural refinement (Fig. 3d, f). The variation of the Seebeck coefficient is in good agreement with that of the electrical resistivity because of the increased carrier concentration. Finally, the bulk sample obtained by SPS of powders subjected to MA at 425 rpm for 20 h shows the highest power factor of $233\ \mu W\ m^{-1}\ K^{-2}$ at 573 K. The thermal conductivity of the sample with the highest power factor ($233\ \mu W\ m^{-1}\ K^{-2}$ at 573 K) was $0.7\ W\ m^{-1}\ K^{-1}$ at 573 K. The ZT value was calculated to be 0.19, which corresponds to a 72% increment as compared with the value of 0.11 we have achieved before.[7] Therefore, optimizing milling conditions to an appropriate energy level, namely appropriate milling speed and milling time, can result in improved TE properties of polycrystalline Bi_2S_3 synthesized using MA plus SPS. Further enhancement of electrical transport properties could be accomplished by optimizing the SPS process, grain orientation, and effective element doping.

CONCLUSIONS

n-Type polycrystalline Bi_2S_3 with high density (>95%) was synthesized by combining the MA and

SPS techniques. Although Bi_2S_3 compound powder can be synthesized easily by the MA process from elemental powders, and no apparent change was found for MA-derived powder when the milling speed and time were changed, the electrical resistivity and thermopower of the resultant Bi_2S_3 samples after SPS varied significantly. Optimizing the MA conditions can greatly reduce the electrical resistivity of the SPS-sintered Bi_2S_3 samples. It was considered that an appropriate amount of sulfur vacancies induced by MA and SPS increases the carrier concentration, but excessive sulfur vacancies reduce the carrier mobility. The maximum power factor reaches 233 μW m^{-1} K^{-2} for the bulk sample obtained from powders ball-milled at optimized conditions of 425 rpm for 20 h, which is the highest value reported so far for bulk Bi_2S_3 samples without texture.

ACKNOWLEDGEMENTS

This work was supported by the National Natural Science Foundation of China (Grant No. 50972012), High-Tech 863 Program of China (Grant No. 2009AA03Z216), and National Basic Research Program of China (Grant No. 2007CB607500).

REFERENCES

1. G. Chen, M.S. Dresselhaus, G. Dresselhaus, J.P. Fleurial, and T. Caillat, *Int. Mater. Rev.* 48, 1 (2003).
2. M. Stordeur, *CRC Handbook of Thermoelectrics*, ed. by D.M. Rowe (Boca Raton: CRC Press, 1995).
3. W. Hofmann, *Z. Kristallogr.* 86, 225 (1935).
4. T.W. Case, *Phys. Rev.* 9, 305 (1917).
5. G. Hodes, J. Manassen, and D. Cahen, *Nature* 261, 403 (1976).
6. B. Chen, C. Uher, L. Iordanidis, and M.G. Kanatzidis, *Chem. Mater.* 9, 1655 (1997).
7. L.D. Zhao, B.P. Zhang, W.S. Liu, H.L. Zhang, and J.F. Li, *J. Solid State Chem.* 181, 3278 (2008).
8. C.J. Tang, G.Z. Wang, H.Q. Wang, Y.X. Zhang, and G.H. Li, *Mater. Lett.* 62, 3663 (2008).
9. S.M. Zhou, *Mater. Lett.* 61, 119 (2007).
10. S.P. Mondal, A. Dhar, and S.K. Ray, *Mater. Sci. Semicond. Process.* 10, 185 (2007).
11. H. Yang, X. Su, and A. Tang, *Mater. Res. Bull.* 42, 1357 (2007).
12. T. Thongtem, A. Phuruangrat, and S. Thongtem, *Mater. Lett.* 61, 3235 (2007).
13. D.P. White and P.G. Klemens, *J. Appl. Phys.* 71, 4258 (1992).
14. L.D. Zhao, B.P. Zhang, J.F. Li, W.S. Liu, and H.L. Zhang, *Solid State Sci.* 10, 651 (2008).
15. C. Suryanarayana, *Prog. Mater. Sci.* 46, 1 (2001).
16. W.S. Liu, B.P. Zhang, and J.F. Li, *Acta Phys. Sin.* 55, 465 (2006).
17. A.M. Ioffe, *Semiconductor Thermoelements and Thermoelectric Cooling* (London: Infosearch Ltd., 1957).